Polymer Degradation and Stability 97 (2012) 88–97

Contents lists available at SciVerse ScienceDirect

Polymer Degradation and Stability

journal homepage: www.elsevier.com/locate/polydegstab

Effect of excimer laser irradiation on crystallinity and chemical bonding of biodegradable polymer

Shan-Ting Hsu*, Huade Tan, Y. Lawrence Yao

Department of Mechanical Engineering, Columbia University, New York, NY 10027, USA

ARTICLE INFO

Article history:
Received 2 August 2011
Received in revised form
13 September 2011
Accepted 6 October 2011
Available online 14 October 2011

Keywords:
Biodegradable polymer
Poly(L-lactic acid)
Laser irradiation
Chemical modification
Crystallinity
Radical mobility

ABSTRACT

The biodegradable polymer such as poly(L-lactic acid) (PLLA) is promising in drug delivery applications because its chemical structure allows it to hydrolyze into non-toxic substances in the human body. In such applications, drugs are embedded in a polymer matrix and released at the rate at which it degrades. PLLA degradation rate is a strong function of its crystallinity. Thus, control over crystallinity allows for continuous modification of drug release profiles. The excimer laser is used in this study to induce surface crystallinity changes because its spatially uniform intensity profile is favorable for surface treatment. The effects of excimer laser irradiation on the surface morphology, crystallinity, and chemical modifications are investigated via optical microscopy, wide-angle X-ray diffraction, and X-ray photoelectron spectroscopy. A model is developed to numerically examine the spatial and temporal temperature profiles, as well as the amount of chemical modifications. It is found that PLLA crystallinity decreases as a function of laser fluence, and that the amount of chemical modifications is minimized by annealing before laser treatment and reducing laser fluences, which decrease free radical mobility and thus the dissociation quantum yield. A working window is demonstrated in which PLLA crystallinity decreases with no measurable chemical modifications, and the working window can be enlarged by decreasing free radical mobility.

1. Introduction

Biodegradable polymers have been attracting wide attention due to their biocompatibility and biodegradability. Being biodegradable, poly(lactic acid) (PLA) is used in food packaging and tissue engineering. Its chemical structure also makes it favorable in drug delivery as it hydrolyzes in the human body into lactic acid, which is then excreted showing no toxicity. In drug delivery, drugs are embedded in a polymer matrix and released as it degrades. The advantages of using biodegradable polymers in drug delivery system can be manifested by the controlled drug release profiles against time [1]. However, due to the induction period of polymer degradation caused by the time for water molecules to penetrate into the matrix, embedded drugs cannot release at the designed rate in the early stage.

Efforts have been made to modify the degradation rate of PLA. Zhao et al. [2] modified its degradation rate by adjusting temperature and pH value in the degradation environment. This attempt is limited since both parameters are invariants in the human body. Blending PLA with another biodegradable polymer, poly(glycolic acid), to adjust the degradation rate is also investigated [3], while the desired properties of PLA may be altered in the copolymer. Tsuji [4] investigate the effects of tacticity, content of L-lactide unit, and blending of poly(L-lactic acid) (PLLA) and poly(D-lactic acid) (PDLA) on the degradation rate of PLA. Although the PDLLA film can have the highest degradation rate, it requires specific chemical reaction environments to synthesize PDLLA with a desired ratio of PLLA and PDLA.

A way to modify PLA degradation rate free from the above limitations is to change its crystallinity [5]. Tsuji and Ikada [6] proposed that PLA degradation begins in the amorphous regions between lamellae, followed by the disorientation of the lamellae and disappearance of the spherulitic structure. Less crystalline regions are expected to degrade faster. Adjusting crystallinity is a relatively simple process, and can be accomplished through thermal treatments such as annealing, melting and quenching [7]. However, they affect the overall properties within the bulk and have limitation since accelerating the initial degradation may only require decreasing surface crystallinity while keeping the bulk intact. Recently, laser irradiation as a heating source to modify the surface crystallinity has drawn increasing attention. It is also attractive due to flexibility, ease of use, and spatial controllability.

* Corresponding author. Tel.: +1 2126662393.
E-mail address: sh2852@columbia.edu (S.-T. Hsu).

0141-3910/$ – see front matter © 2011 Elsevier Ltd. All rights reserved.
doi:10.1016/j.polymdegradstab.2011.10.006

Using the Nd:YAG laser with the photon energy lower than PLLA bond energies, Bhatla and Yao [8] reduced the PLLA crystallinity, and quantified it by the wide-angle X-ray diffraction (WAXD) measurements. However, the non-uniform laser spatial intensity profile makes it difficult to achieve a uniform surface treatment. Because of the incoherent light generated by the excimer laser, the beam can be homogenized without interference, and the homogenized beam is spatially uniform and favorable for surface treatment. Using the excimer laser, Lazare and Benet [9] treat poly(ethylene terephthalate) (PET) films, and demonstrate the presence of a thin amorphous surface layer. Lazare and Benet report that photochemical reactions are possible in addition to photothermal effects, since excimer lasers operate at UV wavelengths with photon energies higher than certain bond energies in polymers. In another attempt to decrease PET film crystallinity using the excimer laser [10], the chemical changes are studied via X-ray photoelectron spectroscopy (XPS). It is found that low fluences cause little chemical changes. These chemical changes include the dissociation of ester bonds and reduce of the number of oxygen atoms due to the emission of small molecules [11]; these modifications could alter the original properties of the polymers.

The primary objective of this work is to reduce crystallinity of PLLA films with excimer laser surface treatment, while minimizing the chemical modifications. The optical microscopy, WAXD, and XPS measurements are utilized to study the morphology, crystallinity, and chemical modifications, respectively. A 2D model considering the thermal and chemical effects is proposed to numerically examine the spatial and temporal temperature profiles and the amount of chemical changes. The effects of radical mobility in the PLLA films and laser fluence have also been considered.

2. Background

2.1. Melting and crystallization

Polymer melting is an amorphization process in which polymer chains detach from crystals, and the crystal dimension decreases longitudinally and transversely [12]. As a rapid process, chain detachment and crystallinity decrease can occur within nanoseconds [13]; melting polymers by a nanosecond laser is thus feasible. The melting temperature T_m of PLLA is between 170 °C and 180 °C. Due to the difference in the fold surface energy σ_e and lateral surface energy of crystals, thicker crystals are more thermodynamically stabile and thus have higher T_m [14,15]:

$$T_m = T_m^0\left(1-\frac{2\sigma_e}{\Delta h_f l}\right) \tag{1}$$

where T_m^0 is the equilibrium melting temperature, Δh_f is the fusion heat, and l is the crystal thickness. Given sufficient chain mobility, lamellar crystals thicken to reduce surface energy. Annealing enhances chain mobility, and can increase l and T_m by 5–10 °C for PLLA [7,16]. Temperatures higher than 200 °C can cause thermal degradation over minutes.

Crystallization begins with the nucleation process. Nucleation of PLLA occurs over minutes. PLLA crystal growth is given by the non-isothermal crystallization kinetics

$$\theta(t) = 1-\exp\left\{-\left[\int_0^t K(T(\tau))\mathrm{d}\tau\right]^m\right\} \tag{2}$$

where $\theta(t)$ is the crystallinity, t is crystallization time, $K(T(\tau))$ is the reaction rate constant, and m is the Avrami exponent. For crystal development t is also on the order of minutes. A cooling rate higher than 50 °C/min prevents molten PLLA from recrystallization [17]. Since laser treatment can induce an extremely high cooling rate, recrystallization during the cooling process of laser treatment does not occur [8].

2.2. Interaction between photons and polymers

Polymer absorption of photons with energies exceeding the bond energy can break the bonds. A series of events is given in Fig. 1 [18]. The photons excite electrons from the ground state *Sg* to the exited state *Se*, Event *1*. Part of the energy is relaxed, Event *2*; part of it breaks the bond, forming free radicals, Event *3*. Some radicals generate decomposed products via Event *4*, while some recombine, Event *5*. Radical reactions release heat. In situations where oxidation does not occur, UV irradiation on PLA breaks the CO bonds in its backbone, separate the CH_3CHCOO units, and generates free radicals R1 and R2 following Eq. (3) [19],

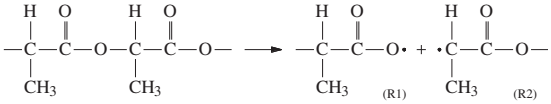

(3)

This reaction occurs between two CH_3CHCOO units. As the reaction continues, the number of scissions increases, which decreases the molecular weight and number of connected CH_3CHCOO units. R1 and R2 can generate smaller molecules such as CO and CO_2 via further reactions [20]. The reactions last for microseconds after the nanosecond UV laser pulse [21]. After laser treatment, bubbles can be observed on the polymer surface [20,22,23].

2.3. Dissociation quantum yield

Competition of Events *4* and *5* in Fig. 1 determines the dissociation quantum yield ϕ, which is the number of dissociations occurring per photon absorbed, defined by

$$\phi = \frac{w}{M_n^0}\frac{d\left(M_n^0/M_n-1\right)}{d\left(N_{ph}t\right)} \tag{4}$$

where w is the sample weight, M_n^0 is the initial molecular weight, M_n is the molecular weight at time t, N_{ph} is the number of absorbed photons per unit time. The number of scissions per chain, M_n^0/M_n-1, increases with radical mobility based on the cage effect. The quantum yield in the mobile state is generally larger by an order under UV irradiation [24], and is proportional to the dissociation reaction rate constant K through [25]

$$K = N_{ph}\sigma(\omega)\phi \tag{5}$$

where $\sigma(\omega)$ is the photon absorption cross section with photon frequency ω.

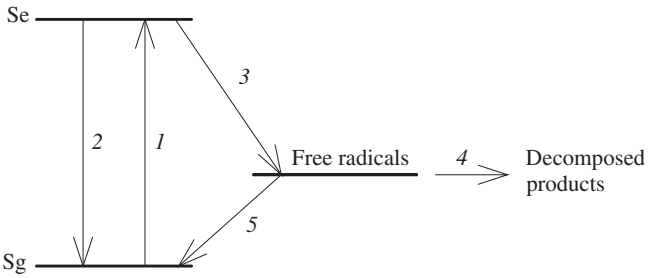

Fig. 1. Elementary events following the polymer absorption of photons with energies higher than the polymeric bond energy.

3. Numerical model

To numerically investigate the spatial and temporal distribution of temperature and the amount of chemical modifications, a 2D symmetric thermal and chemical model is developed. Since PLLA is semitransparent at UV, laser irradiation energy is absorbed by the bulk, and the bulk temperature is governed by the heat equation

$$\rho C_p(T)\frac{\partial T}{\partial t} = \nabla\cdot(k\nabla T) + q(z,t) + q_{rad} \tag{6}$$

where ρ is density, $C_p(T)$ is specific heat, k is conductivity, z is laser irradiation depth, $q(z, t)$ is the laser power density, and q_{rad} is the release heat of radical reactions and will be determined in Eq. (12). For an incompressible material, change in $C_p(T)$ during the phase transition can be approximated by $\Delta C_p = \Delta h_f/T_m$, where Δh_f is the heat of fusion. The specific heat is calculated as

$$C_p(T) = C_{p0} + \Delta C_p U(T - T_m, \Delta T) \tag{7}$$

where C_{p0} is the specific heat in the solid state and U is a step function with value 0 for $T \le T_m - \Delta T$ and 1 for $T \ge T_m + \Delta T$. The specific heat of polymeric materials is typically around 1000 J/(kg K) [26]; thus C_{p0} is assumed 1000 J/(kg K). ΔT, 10 °C, is half the transition temperature span. Laser power density, $q(z, t)$, is a function of space and time

$$q(z,t) = A\cdot q_0\cdot\exp(-\alpha z)\cdot\exp\left[-4\ln 2\left(\frac{t-2t_p}{t_p}\right)^2\right] \tag{8}$$

where A is the absorptivity, 0.07, α is the absorption coefficient, 10^3 cm^{-1} [27], t_p is the pulse width, 25 ns, and q_0 is the peak power density obtained by $q_0 = \alpha F/t_p$ with F the laser fluence. Convection and radiation are considered on the boundaries while insulation is specified along the symmetry line. The initial temperature is set 20 °C. Change of crystal size due to annealing is not of interest, while its effect on T_m is considered by assuming different T_m's for the non-annealed films (175 °C) and annealed films (180 °C). From the backgrounds of crystallization and cooling rate in Sec. 2.1, it is assumed that no crystallization occurs during cooling; the assumption will be validated by our simulation results in Sec. 5.2. Crystallinity decreases as the material melts; therefore, the crystallinity change is related to the melting depth in the film.

The chemical modifications occur via Eq. (3) if R1 and R2 do not recombine. The amount of modifications depends on the number of scissions, Eq. (4). As scission occurs, the connections of the CH_3CHCOO units at their ester group with another unit are broken, and the number of such connected CH_3CHCOO units decreases. Therefore, the number of the CH_3CHCOO units with connection at their ester group to another unit in a unit volume, or its number density, is modeled. For incompressible materials, the number density is governed by the mass conservation equation

$$\frac{\partial c}{\partial t} + \boldsymbol{u}\cdot\nabla c = \nabla\cdot(D\nabla c) + r \tag{9}$$

where c is the number density with an initial value of c_0, $\boldsymbol{u}$ is the velocity vector, D is the diffusion coefficient, and r is the reaction rate. Velocity and diffusion gradients are assumed to be negligible during laser treatment, and thus $\partial c/\partial t = r$. The reaction rate is given by the crystallinity θ,

$$r = \theta\cdot r_c + (1-\theta)\cdot r_a \tag{10}$$

where r_c and r_a are the reaction rates of the crystalline and amorphous domains, respectively. The photochemical reaction rate is proportional to the number density [28]. Thus, $r_c = c\cdot K_c$ and $r_a = c\cdot K_a$ where K_c and K_a are the reaction rate constants of the crystalline and amorphous domains, respectively. Temperature dependence of reaction rate is expressed by the Arrhenius expressions for the reaction rate constant [29]; the proportionality between the reaction rate constant and quantum yield [25] is also considered.

$$K_i = K_0\cdot\exp\left(-\frac{E}{RT}\right)\cdot\phi_i \tag{11}$$

where $i = c$ or a and K_0 is the pre-exponential factor of the Arrhenius expression, assumed 10^7 1/s, E is the activation energy, assumed 25 kJ/mol, and R is the universal gas constant. ϕ_c and ϕ_a are the step functions accounting for the quantum yields in solid and mobile states. To consider the one-order-of-magnitude difference of the quantum yields in the mobile and solid states [24], ϕ_c is assumed 1 if $T > T_m$ and 0.1 if $T \le T_m$ and ϕ_a is assumed 1 if $T > T_g$ and 0.1 if $\le T_g$. Temperature is imported from the thermal analysis. It is assumed that the time period for the photochemical process (t_{deg}) is 20 μs and that no flux across the boundaries. The release heat of radical reactions q_{rad} is considered as

$$q_{rad} = \left(\frac{c_{rad}}{2}\right)\left(\frac{H_{rad}}{t_{deg}}\right)U_{rad} \tag{12}$$

where c_{rad} is the number density of the free radicals to be recombined or react, which is $2c$ if all molecules in the ground state can be excited to generate free radicals (Event *1* in Fig. 1). Also in Eq. (12), H_{rad} is the reaction heat by each event, around 600 J/mol [30], and U_{rad} is the step function whose value is 1 if $t \le t_{deg}$ and 0 if $t > t_{deg}$ to consider the time period of the photochemical process. The reaction heat is then output to the thermal analysis. Part of the crystalline chain becomes amorphous during melting, while its motion could be constrained by surrounding crystals. Thus, at the same T, the initial crystalline domain is assumed to have the same mobility and reaction rate before and after melting. Since the amount of chemical modifications on the polymer chains induced via Eq. (3) is of interest and the generated free radicals only react with other radicals instead of the polymer chains [20], the subsequent chemical reactions and products are not considered in the simulation.

The coupled partial differential Eqs. (6) and (9) with boundary and initial conditions can be solved through the finite element method. The software COMSOL Multiphysics 4.1 is used. A 2D symmetric model is developed and composed of thermal and chemical analyses. Its domain is 0.7 mm × 20 μm with laser beam size 0.5 mm. The thermal analysis is realized by the Heat Transfer in Solids Interface of the Heat Transfer Module. The chemical analysis is accomplished by the Transport of Diluted Species Interface of the Chemical Reaction Engineering Module, which is able to compute the number density of a single species under varying reaction rates. The COMSOL smoothed Heaviside function, *flc2hs*, is used as the step functions.

4. Materials and methods

PLLA granules were provided by PURAC and used as received. The inherent viscosity of PLLA in chloroform at 25 °C is 1.6 dl/g, and the molecular weight is thus estimated as 5.6 × 10^4 g/mol [31]. Films were prepared by the solvent casting method described in reference [32]. The film thickness is 20–25 μm. Dissociation quantum yield changes with radical mobility, which can be reduced by higher crystallinity. Annealing increases crystallinity, and can obtain films with lower radical mobility when radicals are formed due to laser irradiation. Non-annealed films are termed films with high radical mobility. Annealing is conducted at 140 °C for 1 h. A KrF excimer laser with wavelength 248 nm and pulse width 25 ns is

used. The homogenized laser beam has spatially uniform intensity favorable for a uniform surface treatment. The film is radiated by a single pulse with fluence 1.80 J/cm^2 to 2.80 J/cm^2 in argon atmosphere with the flow rate of 15 standard cubic feet per hour to prevent oxidation. Morphology of PLLA films is observed via optical microscopy. WAXD measurement is accomplished using the Inel X-ray diffractometer. Monochromatic CuKα radiation with wavelength 0.15418 nm at 40 kV and 30 mA is used. X-ray photoelectron spectroscopy (PHI 5500 ESCA) is used to analyze chemical constituents of pre- and post-treated films. The O_{1s} and C_{1s} spectra are captured, and the take-off angle is 45°.

5. Results and discussion

5.1. Effects of laser irradiation on morphology

The morphologies of the laser treated films are given in Fig. 2(a)–(d). High fluence irradiation generates appreciable bubbles as a result of laser energy penetration into the bulk due to the low absorption coefficient (10^3 cm^{-1}) of PLLA at UV wavelength. The same phenomenon has been reported in poly(methyl methacrylate) (PMMA) under the excimer laser irradiation [22,23]. Its absorption coefficient is on the same order as PLLA, and the fluences of several J/cm^2 generate bubbles in both materials.

The bubble formation in laser treated polymers has been explained by different theories. Srinivasan [33] suggests that the bubbles are the gas trapped by the melted and re-solidified material, while others believe that the bubbles are the gaseous products from the decomposition of original materials [22]. The origin of bubble formation can be revealed by comparing the morphology shown in Fig. 2 and the XPS results shown in Figs. 8–10. (The XPS measurements and chemical modifications will be discussed in more detail in Sec. 4.3.) Fig. 2 shows that appreciable bubbles are generated in the film with high radical mobility if the fluence achieves 2.60 J/cm^2 (Fig. 2(b)). However, in the film with low radical mobility, the appreciable bubbles form only when the fluence reaches 2.70 J/cm^2 (Fig. 2(d)). The results agree with the XPS measurements, which show that appreciable chemical modifications occur at 2.60 J/cm^2 and 2.65 J/cm^2 for the film with high and low radical mobility, respectively. Thus, bubble formation is believed to be a chemical process involving the decomposition of the original material. The components in the bubbles include small molecules such as CO and CO_2 [20].

Laser fluences used in this study are on the order of J/cm^2, while the fluences treating PET are only several mJ/cm^2 [9,10]. This difference comes from different absorption coefficients of PET (10^5 cm^{-1}) and PLLA at UV wavelength [27], which determines the laser penetration depth. The penetration depth, defined as the depth at which the laser intensity in the bulk falls to $1/e$ of the original intensity, is the reciprocal of the absorption coefficient based on the Beer–Lambert Law. The penetration depth is on the order of 0.1 μm for PET and 10 μm for PLLA. Therefore, PET concentrates laser energy on the surface, reducing fluences required to induce surface modification, while PLLA allows larger energy penetration and higher fluences are needed to modify the material.

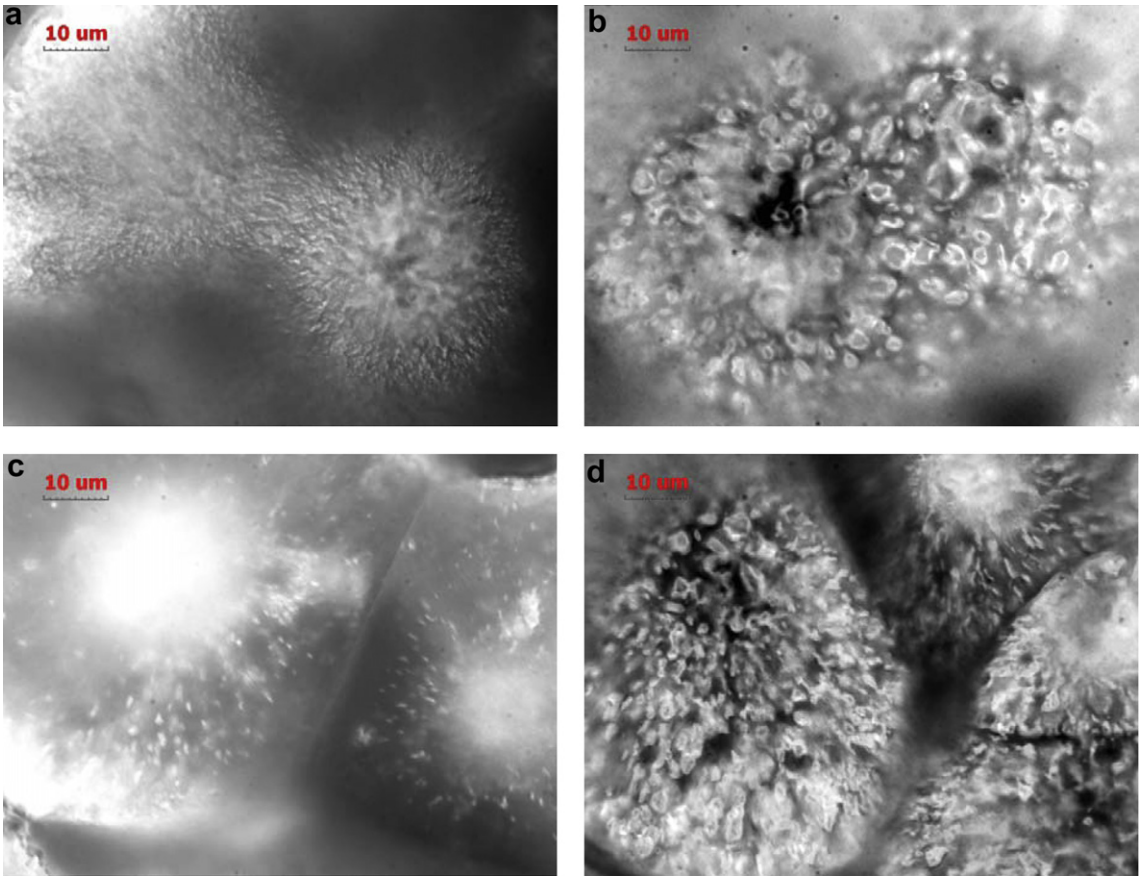

Fig. 2. Morphologies of the film with high radical mobility treated with fluence of (a) 2.50 J/cm^2 and (b) 2.60 J/cm^2, and film with low radical mobility treated with fluence of (c) 2.60 J/cm^2 and (d) 2.70 J/cm^2.

5.2. Decrease of crystallinity by laser irradiation

Crystallinity is investigated via WAXD, and the results for the films with high radical mobility are given in Fig. 3. The peaks become less prominent for the films treated with higher fluences, suggesting a lower crystallinity. Similar results are obtained for the films with low radical mobility, while more prominent peaks are observed due to its higher crystallinity caused by annealing. The crystallinity is calculated based on reference [34] with results given in Fig. 4. Fig. 4 quantitatively shows that annealing results in a higher crystallinity; radical mobility may thus be reduced. It is also shown in Fig. 4 that crystallinity decreases at a certain fluence, which suggests a thermal process involving polymer melting.

From Fig. 4, the crystallinities of the two kinds of films both decrease at 2.30 J/cm^2, suggesting that the increase of T_m due to annealing does not affect the onset of crystallinity decrease. This is because the temperature increment caused by different fluences is larger than the T_m difference caused by annealing. However, the T_m difference causes different amount of crystallinity change. For the film with high radical mobility (the non-annealed film), crystallinity decreases from 31% to 14% after treated with a 2.70 J/cm^2 pulse, which is 55% decrease. For the film with low radical mobility (the annealed film), the crystallinity decreases from 48% to 34% under the same condition, which accounts for 29% decrease. Namely, less amount of material is melted in the annealed film. Since WAXD measures the crystallinity in the bulk due to the high penetration depth of X-ray, a possible scenario is that the lower T_m in the non-annealed film facilitates melting, and thus the amount of crystallinity decrease is larger.

To numerically investigate the temperature distribution and melting depth in the film, a 2D thermal model is developed. A typical temperature distribution is given in Fig. 5. The highest temperature occurs on the surface due to the highest local laser energy density, and the temperature decreases with depth. Since the excimer pulse intensity is spatially uniform, the temperature distribution is not a function of the distance to the beam center.

The melting depth is also determined from the simulation results, as given in Fig. 6. For both kinds of films, melting begins once the fluence reaches a certain level (2.10 J/cm^2 in the simulation), and melting depth increases with fluence thereafter. The simulation agrees with the WAXD measurements in that small difference in T_m of both films does not affect the onset of melting.

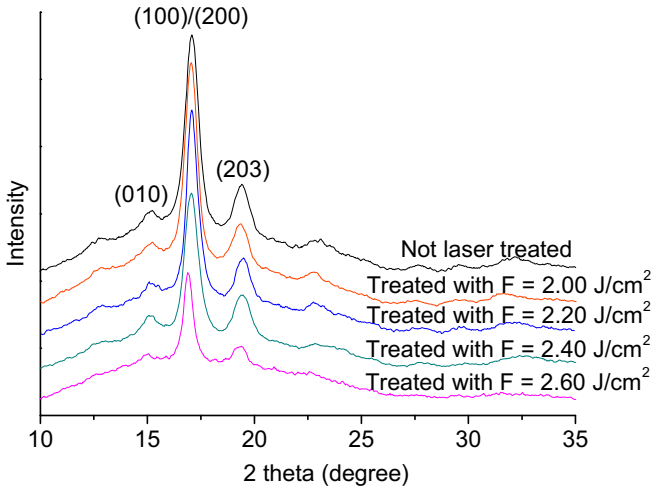

Fig. 3. WAXD profiles of crystalline PLLA films with high radical mobility before and after laser treatment. Note that the peaks decrease at higher fluences (2.40 and 2.60 J/cm^2). The same trend is observed for the films with low radical mobility.

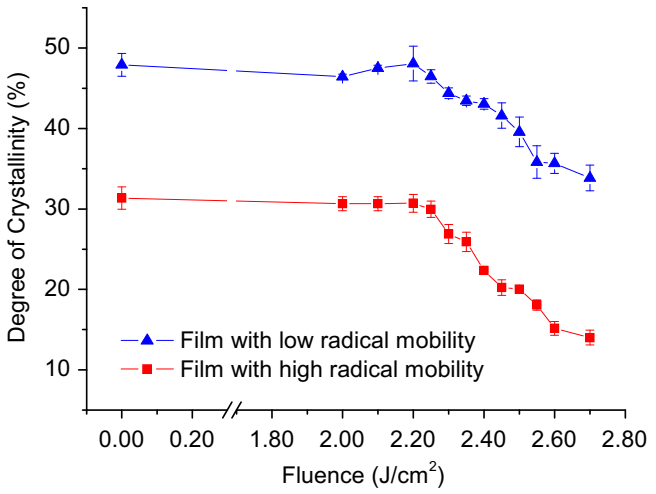

Fig. 4. Crystallinity of PLLA films derived from the WAXD results as a function of laser fluence.

Simulation results confirm that crystallinity decreases from the surface, and that different melting depths are obtained with different T_m's. The non-annealed film has larger melting depth because of its lower T_m, which in turn allows crystallinity to decrease at a larger extent, as observed in the WAXD. Therefore, the amount of crystallinity decrease is a bulk phenomenon and can be explained by the melting depth in the film.

To determine the cooling rate after the laser pulse, the temperature time history is obtained from the model. A typical result is given in Fig. 7, which describes the temperature time history on the surface of the film with low radical mobility treated with 1.80 and 2.80 J/cm^2. It is observed that the temperature drops below T_g at a cooling rate of 10^5 °C/min. At temperatures lower than T_g, the structure becomes solid and no crystallization can occur. Since a cooling rate higher than 50 °C/min prevents PLLA recrystallization [17], recrystallization does not occur in our case, as agrees with reference [8] and our assumption. The temperature can exceed the thermal degradation temperature (~200 °C) due to laser irradiation. However, thermal degradation requires minutes to occur [35] and therefore is negligible during this rapid cooling process.

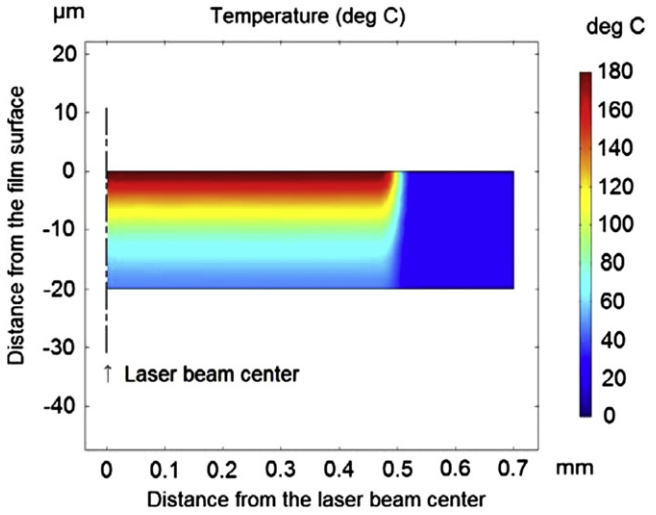

Fig. 5. Simulation result of the typical temperature distribution in the film. This simulation depicts the film with high radical mobility 1 μs after the onset of a 2.40 J/cm^2 laser pulse.

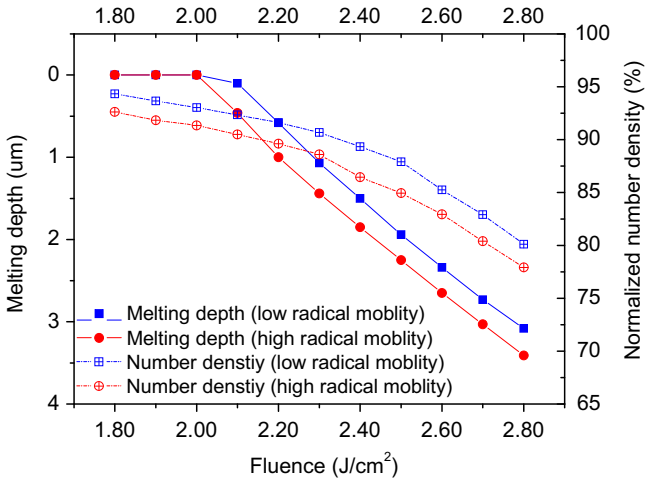

Fig. 6. Simulation results of the melting depth in the film and the normalized number density of the CH_3CHCOO units connecting at their ester group with other CH_3CHCOO units.

5.3. Chemical modifications

5.3.1. Modifications of chemical bonds

XPS measurements are performed to investigate the chemical modifications on the film surface. O_{1s} and C_{1s} spectra are recorded to determine the amount of O and C elements and possible bond breakages. C_{1s} spectra of the film with high radical mobility before and after laser treatment are given in Fig. 8(a)–(c). The profiles are composed of three peaks, which come from the three carbon groups in the structure: the C–H groups, the C–O groups in the backbone, and the O–C=O groups in the ester bonds. They have the binding energies of 285, 287, and 289 eV, and contribute to Peak 1, Peak 2, and Peak 3, respectively [36]. The resolved peaks are also given in Fig. 8. It is observed that the profiles remain similar until a high fluence is utilized.

Areas under the resolved peaks in Fig. 8 are calculated. The calculation results are shown in Fig. 9(a)–(b) for both kinds of films as a function of laser fluence. Peak areas change only when the laser fluence reaches certain levels, which are 2.60 J/cm^2 and 2.65 J/cm^2 for the film with high and low radical mobility, respectively. The

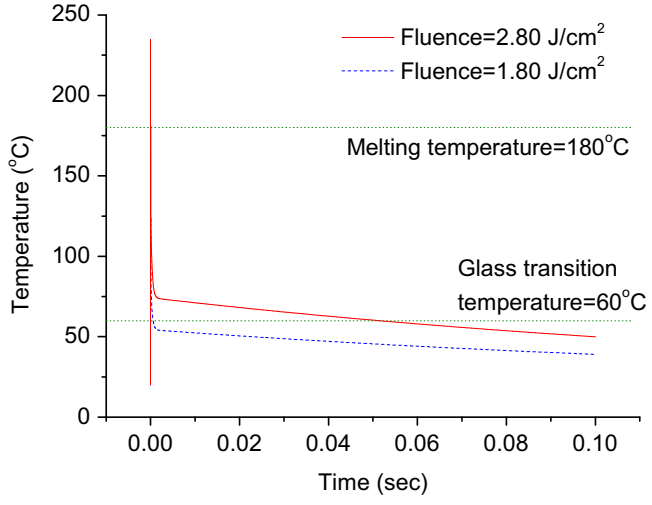

Fig. 7. Simulation result of the typical film temperature profiles as a function of time after laser irradiation. The simulation predicts the temperature profile on the surface of the film with low radical mobility treated a single pulse with fluence of 1.80 and 2.80 J/cm^2.

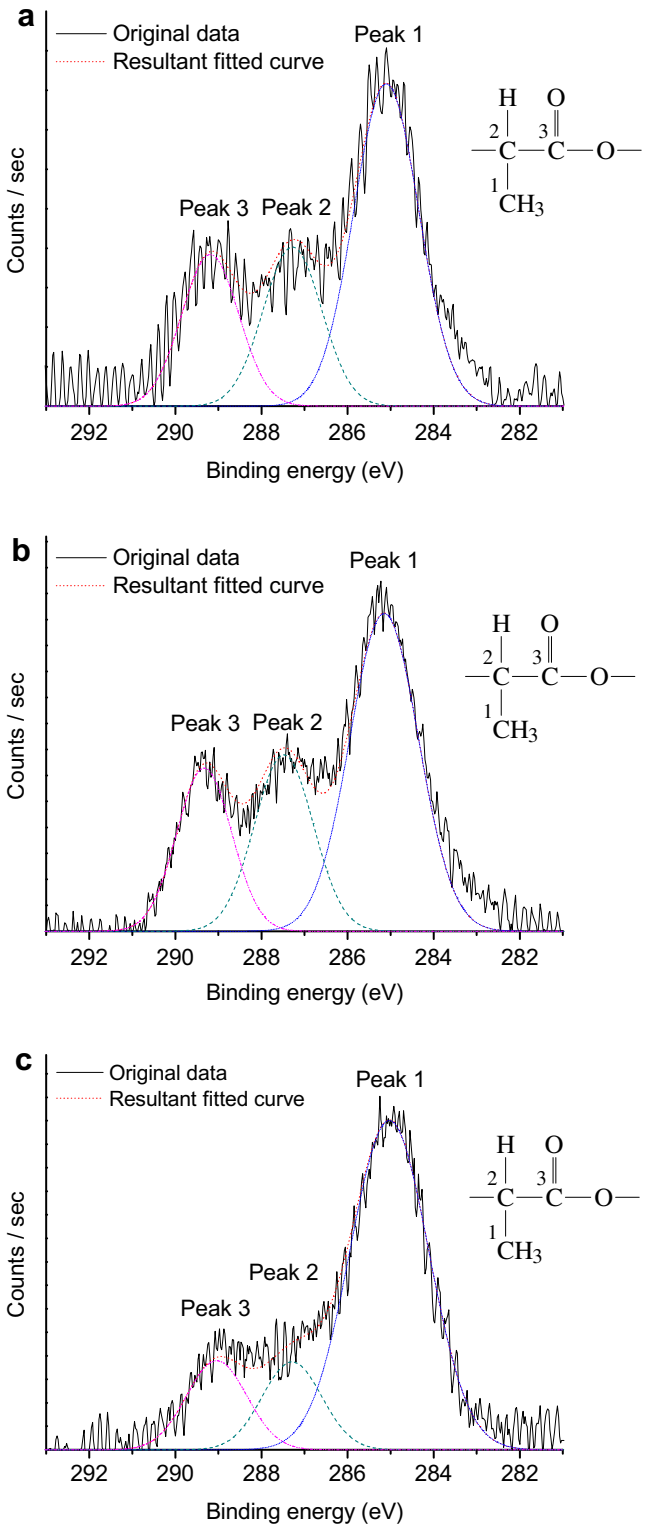

Fig. 8. Typical C_{1s} XPS spectra and the resolved peaks of the film before and after laser treatment. The figures show the results of the film with high radical mobility (a) before laser treatment, and treated with fluences of (b) 2.50 J/cm^2 and (c) 2.60 J/cm^2. Note that the peak area ratio does not agree with the theoretical value, 1:1:1; a possible reason is given in Sec. 5.3.1.

excimer laser used in this study generates photons with 248-nm wavelength, whose energy is 5.0 eV. Chemical bond energies in PLLA are 3.6 eV for the C–C bonds, 3.8 eV for the C–O bonds, 7.5 eV for the C=O bonds, and 4.3 eV for the C–H bonds. Since the

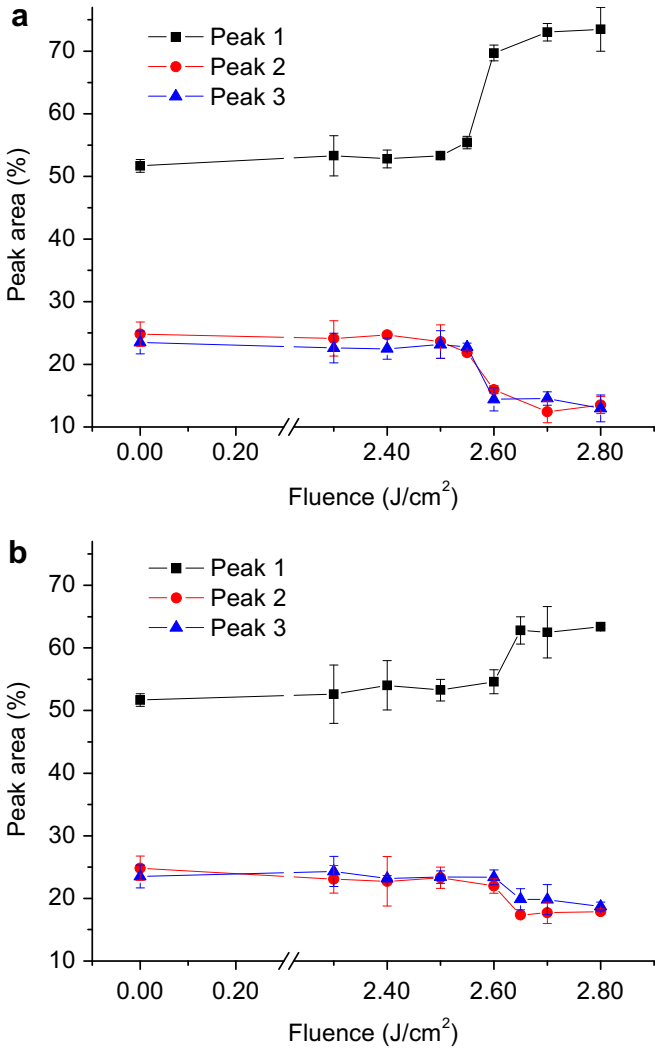

Fig. 9. Area percentage of the three resolved peaks in the C_{1s} XPS spectra of the films with (a) high radical mobility and (b) low radical mobility.

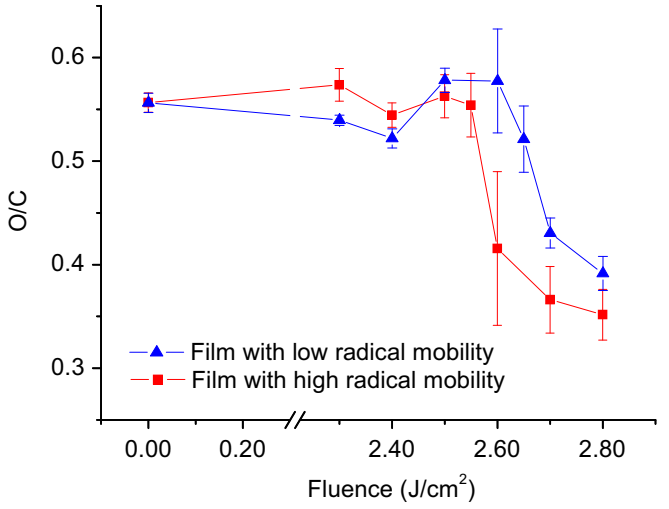

Fig. 10. Ratio of the O_{1s} peak area to the C_{1s} peak area derived from the XPS spectra for the films with high and low radical mobility.

photochemical reactions occur whenever the energy of a single photon exceeds the dissociation energy, chemical bond breakage always occurs. The threshold behavior shown in the XPS results thus suggests that low-fluence laser treatment induces an insignificant amount of chemical modifications not reflected in the measurements [10].

XPS results also reveal possible chemical reactions. Decrease of Peaks 2 and 3 in Fig. 9 suggests, respectively, the loss and/or breakage of the C–O groups in the backbone and the O–C=O groups in the ester bonds. The O/C ratio decreases shown in Fig. 10 suggests the loss of oxygen atoms. Since bubbles are composed of small gaseous products from chemical decomposition as discussed in Sec. 5.1, a portion of the oxygen atoms is believed to emit from the film in form of CO and CO_2. A possible series of chemical reactions following the generation of the free radicals R1 and R2 through Eq. (3) is given in Appendix [20]. The generation of R1 and R2 via Eq. (3) requires the breakage of the C–O bonds in the backbone, which reduces the amount of the carbon atoms contributing to Peak 2. Due to the instability of R1 and R2, two R1's may react to produce R3 and CO_2 following Eq. (A.1). The evolution of CO_2 decreases the amount of oxygen atoms as well as the carbon group accounting for Peak 3. Two R3's may react to generate R4 and eliminate small molecules CHO–CH_3 through Eq. (A.2). R4 may decompose into R3 and CO through Eq. (A.3), forming a chain reaction. Two R2's may react to produce R5 and C_2H_4 through Eq. (A.4). R5 can further decompose into R2 and CO_2 through Eq. (A.5); this further decreases the amount of oxygen and the area under Peak 2, and also initiates a chain reaction between R2 and R5.

It is noticed that the area under Peak 1 is larger than those under Peaks 2 and 3, and the peak area ratio does not agree with the theoretical value, 1:1:1. The theoretical value of the peak area I can be determined through the equation

$$I = K_0 N_a \sigma_c \lambda_p A_s T_a \tag{13}$$

where K_0 is the instrument constant, N_a is the atomic concentration, σ_c is the photoionization cross section for an element, λ_p is the inelastic mean-free path length for photoelectrons, A_s is the area of the sample, and T_a is the analyzer transmission function. Sample area A_s, being a constant, is not expected to cause the deviation from the theoretical value. σ_c and λ_p depend on chemical elements and do not cause the deviation since the element of interest is carbon. Both K_0 and T_a are device dependent constants and are not the cause either. Atomic concentration N_a can be the reason. Larger area of Peak 1 suggests a higher concentration of the side group CH_3 on the surface than the other two carbon groups in the backbone. Since XPS is sensitive to a monolayer of atoms on the surface, the side group is believed to be more abundant on the surface. This abundance could be due to the fact that the crystalline chains are well-aligned in the lamellae, and their side groups uniformly protrude outward from the chains. Such side groups may form the outmost atom layer on the lateral surface of the lamellae, and thus the surface of spherulites and the film. Therefore, in the ordered structure the side group may have higher concentration on the film surface. The explanation is supported by a separated XPS measurement on an amorphous PLLA film prepared by spin coating with procedures detailed in reference [32]. Results of both area ratio and atomic ratio O/C (not shown) agree with the theoretical values, since the distribution of the three carbon groups is more uniform in a less ordered structure.

5.3.2. Effect of radical mobility on the amount of chemical modifications

The amount of chemical modifications can be revealed by the XPS results given in Figs. 9 and 10, which show that appreciable

chemical modifications occur at a lower fluence (2.60 J/cm^2) for the film with high radical mobility and higher fluence (2.65 J/cm^2) for the film with low radical mobility. Peak areas and the O/C ratios also change more for the film with high radical mobility. To numerically investigate the amount of chemical modifications, the number density of the CH_3CHCOO units connecting at their ester group with another unit is simulated and represented in terms of normalized values based on the initial number density c_0 in Eq. (9). The normalized number density is thus defined as $c/c_0 \times 100\%$ and represents the percentage of the initial value c_0. The normalized number density of the film with high radical mobility is given in Fig. 11, which shows that the number density decreases with time and fluence. The same trends are obtained for the film with low radical mobility. The simulation is computed for the film surface and thus comparable with the XPS results. The normalized number density is also plotted as a function of fluence as given in Fig. 6, which shows that the film with high radical mobility experiences more chemical modifications under the same fluence, as agrees with the XPS results.

The reason that the film with less radical mobility has less chemical modifications is because radicals with low mobility less easily react with other free radicals to generate decomposed products. This is known as the cage effect, which states that the free radicals generated by the dissociation of molecules are unable to move apart due to the existence of surrounding molecules, with the result that the dissociation products may recombine and return to the initial state. To react with each other it is required that the free radicals meet in a single cage, which is the volume in which the probability of reaction is significantly higher. The cage radius is affected by radical mobility, which is higher in a high temperature or the molten state. The cage radius can reach several tens of angstroms at a temperature close to the melting temperature [37]. Due to a large cage radius, the radicals have high possibility to react with other radicals within the cage. When the radical mobility is hindered, such as in the crystalline domain, the effective cage radius decreases to the dimension of the elementary crystal unit cell, and the number of active radicals in the cage is much less. Free radicals can also diffuse from cage to cage to react with others. However, the diffusion is slow in a polymer matrix with a diffusion coefficient on the order of 10^{-15} to 10^{-18} cm^2/s. This slow process leads to a high probability of free radical pair recombination in the cage, which is dominant in the crystalline domain. This accounts for the phenomenon that higher fluence is required to cause chemical modifications in the film with high radial mobility and its larger amount of chemical modifications.

Fig. 6 shows that chemical modifications always occur even at small fluences, and no chemical modification threshold exists. This differs from the XPS results while agrees with the photochemical decomposition theory. The threshold observed in the XPS measurements, Figs. 8–10, is due to insignificant amount of chemical modifications. Appreciable amounts of chemical modifications are generated by higher fluences. Chemical changes obtained from experiments tend to level off at high fluences, while in the simulation the trend becomes steeper. Small molecules generated by laser irradiation are ejected from the surface and are not detected by the XPS measurements. However, the molecular ejection is not considered in the model, which causes the steeper trend of chemical change in the simulation results.

The reaction rate of Eq. (3), r, defined in Eq. (9) as $\partial c/\partial t$, is determined. Fig. 12 gives its absolute value for the amorphous domain on the surface of the film with high radical mobility; similar trends are obtained for the film with low radical mobility. The amorphous domain becomes mobile as the temperature reaches T_g, which is 60 °C for PLLA. During the period when the photodegradation can last, the temperature remains higher than T_g. Therefore, the amorphous domain is in mobile state and has a high quantum yield according to the cage effect. The dissociation rate is maintained on the order of 10^6 mol/(m^3 s). The rate changes with temperature and thus increases with fluences and decreases exponentially with time.

Fig. 13 gives the absolute value of the reaction rate for the original crystalline domain on surface of the film with high radical mobility. The crystal structure becomes mobile as the temperature increases up to T_m, which is assumed 175 °C for the film with high radical mobility and 180 °C for the film with low radical mobility due to annealing. The temperature exceeds T_m because of high laser fluences and subsequently drops below it. When the temperature is higher than T_m, the crystals are melted and the dissociation rate is significantly increased due to the high free radical mobility. The rate is maintained around 10^6 mol/(m^3 s) as in the amorphous structure, Fig. 12. As the temperature drops below T_m, radical mobility is limited by the remaining crystal structure, and is assumed to be that of the crystal structure. The dissociation rate drops to the order of 10^5 mol/(m^3 s). However, for smaller fluences, 1.80, 1.90, and 2.00 J/cm^2 for both films, the dissociation rate is kept on the order of 10^5 mol/(m^3 s). At these fluence levels, no surface

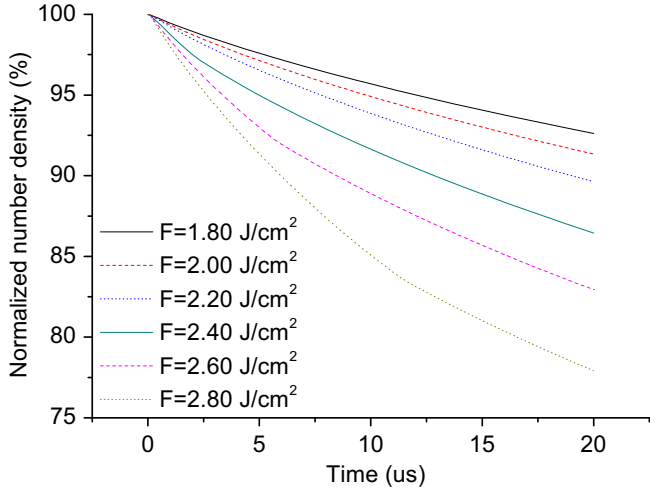

Fig. 11. Simulation results of the typical normalized number density of the CH_3CHCOO units connecting at their ester group with other CH_3CHCOO units on the surface. Results of the film with high radical mobility are shown.

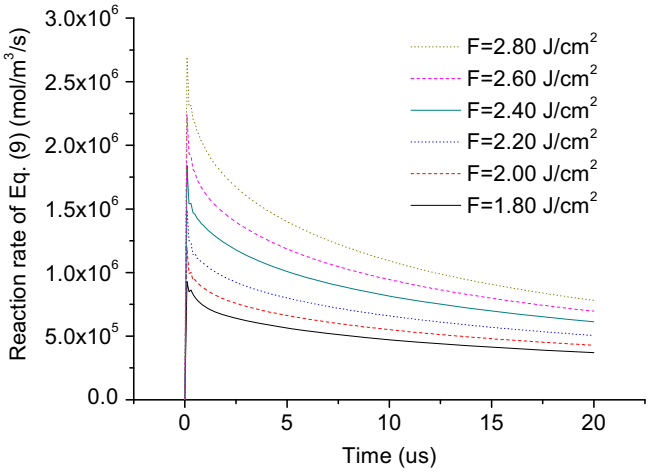

Fig. 12. Simulation results of the typical absolute value of the reaction rate of Eq. (9) for the amorphous domain after the onset of laser pulse. Results of the film with high radical mobility are shown.

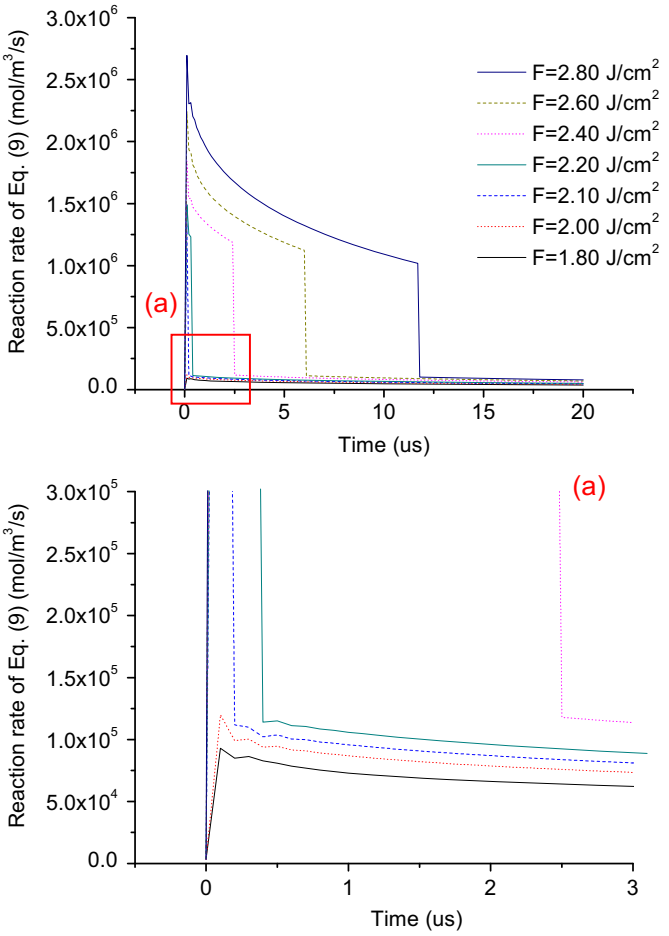

Fig. 13. Simulation results of the typical absolute value of the reaction rate of Eq. (9) for the crystalline domain after the onset of laser pulse. Results of the film with high radical mobility are shown.

melting occurs under these fluences, and mobility is therefore low. The results also agree with the simulated melting depth, Fig. 11, which demonstrates that 2.10 J/cm^2 is the lowest fluence causing surface melting for both films. Similar trends are obtained for the film with low radical mobility, while the dissociation rate maintains at higher value for a shorter time. A fluence of 2.80 J/cm^2 maintains a high dissociation rate for the film with high radical mobility for 12 μs, while it only maintains for 9 μs for another type of film. The film with low radical mobility, due to annealing, has a higher T_m, and therefore temperature drops below the T_m sooner.

6. Conclusions

PLLA crystallinity changes and chemical modifications under excimer laser irradiation are experimentally and numerically investigated. Crystallinity decrease due to laser melting is demonstrated, and the effects of radical mobility on chemical modifications are evaluated. The amount of chemical modifications is determined by the free radical mobility, which is decreased by increasing the crystallinity through annealing before laser treatment. Both the WAXD and simulation results show that the decrease of crystallinity initiates at the same fluence for both films with high and low radical mobility. According to the XPS measurements and simulation, the film with low radical mobility has a smaller amount of chemical modifications, and larger fluences are required to cause appreciable chemical modifications. Films with smaller radical mobility have a larger working window, in which the surface melting occurs while the chemical modifications are limited. A larger working window increases the applicability of surface treatment by the excimer laser.

Acknowledgements

Financial support from NSF under CMMI-1030536 is acknowledged. WAXD and XPS measurements were carried out at MRSEC, Columbia University.

Appendix

A possible series of chemical reactions following generating the free radicals R1 and R2 by UV laser irradiation through Eq. (3) is given as follows [20].

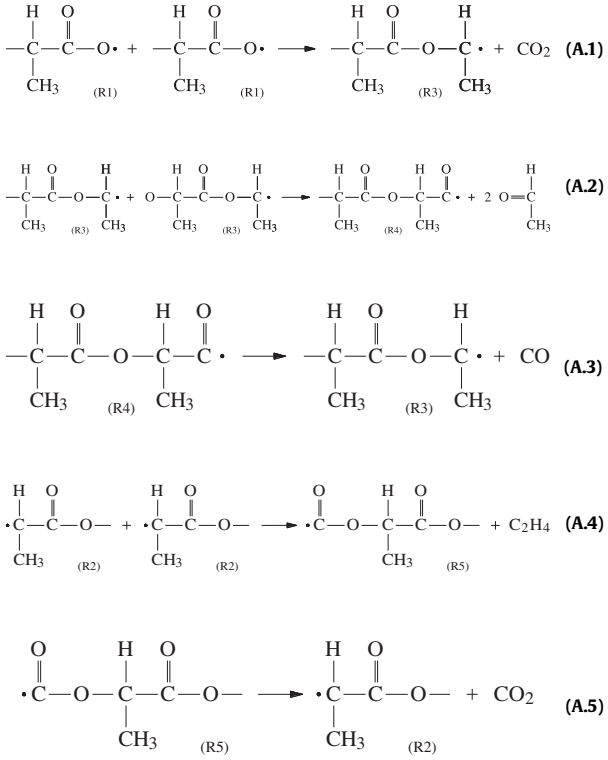

References

[1] Amass W, Amass A, Tighe B. A review of biodegradable polymers: uses, current developments in the synthesis and characterization of biodegradable polyesters, blends of biodegradable polymers and recent advances in biodegradation studies. Polym Int 1998;47:89–144.
[2] Zhao Y, Fu J, Ng DKP, Wu C. Formation and degradation of poly(D, L-lactide) nanoparticles and their potential application as controllable releasing devices. Macromol Biosci 2004;4:901–6.
[3] Miller RA, Brady JM, Cutright DE. Degradation rates of oral resorbable implants (polylactates and polyglycolates): rate modification with changes in PLA/PGA copolymer ratios. J Biomed Mater Res 1977;11:711–9.
[4] Tsuji H. Autocatalytic hydrolysis of amorphous-made polylactides: effects of L-lactide content, tacticity, and enantiomeric polymer blending. Polymer 2002; 43:1789–96.
[5] Nampoothiri KM, Nair NR, John RP. An overview of the recent developments in polylactide (PLA) research. Bioresour Technol 2010;101:8493–501.
[6] Tsuji H, Ikada Y. Properties and morphology of poly(L-lactide). II. hydrolysis in alkaline solution. J Polym Sci, Part A: Polym Chem 1998;36:59–66.
[7] Tsuji H, Ikada Y. Properties and morphology of poly(L-lactide). 1. Annealing condition effects on properties and morphologies of poly(L-lactide). Polymer 1995;36(14):2709–16.

[8] Bhatla A, Yao YL. Effect of laser surface modification on the crystallinity of poly(L-lactic acid). J Manuf Sci Eng 2009;131:051004.
[9] Lazare S, Benet P. Surface amorphization of mylar films with the excimer laser radiation above and below ablation threshold: ellipsometric measurements. J Appl Phys 1993;74(8):4953–7.
[10] Dunn DS, Ouderkirk AJ. Chemical and physical properties of laser-modified polymers. Macromolecules 1990;23:770–4.
[11] Watenabe H, Takata T, Tsuge M. Polymer surface modification due to excimer laser radiation—chemical and physical changes in the surface structure of poly(ethylene terephthalate). Polym Int 1993;31:247–54.
[12] Belyayev OF. Mechanism of melting of oriented polymers. Polym Sci U.S.S.R 1988;30(11):2545–52.
[13] Yamamoto T. Molecular dynamics of reversible and irreversible melting in chain-folded crystals of short polyethylene-like polymer. Macromolecules 2010;43:9384–93.
[14] Cormia RL, Price FP, Turnbull D. Kinetics of crystal nucleation in polyethylene. J Chem Phys 1962;37(6):1333–40.
[15] Hoffman JD, Weeks JJ. Melting process and the equilibrium melting temperature of polychlorotrifluoroethylene. J Res Natl Bur Stand-A Phys Chem 1962; 66A(1):13–28.
[16] Mitomo H. Correspondence of lamellar thickness to melting point of nylon-6,6 single crystal. Polymer 1988;29:1635–42.
[17] Di Lorenzo ML. Crystallization behavior of poly(L-lactic acid). Eur Polym J 2005;41:569–75.
[18] Lazare S, Granier V. Ultraviolet laser photoablation of polymers: a review and recent results. Laser Chem 1989;10:25–40.
[19] Janorkar AV, Metters AT, Hirt DE. Degradation of poly(L-lactide) films under ultraviolet-induced photografting and sterilization conditions. J Appl Polym Sci 2007;106:1042–7.
[20] Inagaki N, Narushima K, Tsutsui Y, Ohyama Y. Surface modification and degradation of poly(lactic acid) films by Ar-plasma. J Adhes Sci Technol 2002; 16(8):1041–54.
[21] Schneider S, Richter F, Brem B. The photodegradation of poly(2,6-dimethyl-1,4-phenylene oxide)—a flash photolysis study of polymer and model compounds. Polym Degrad Stab 1998;61:453–64.
[22] Rebollar E, Bounos G, Oujja M, Georgiou S, Castillejo M. Effect of molecular weight on the morphological modifications induced by UV laser ablation of doped polymers. J Phys Chem B 2006;110:16452–8.
[23] Efthimiopoulos T, Kiagias H, Christoulakis S, Merlemis N. Bubble creation and collapse during excimer laser ablation of weak absorbing polymers. Appl Surf Sci 2008;254:5626–30.
[24] Dan E, Guillet JE. Photochemistry of ketone polymers. X. Chain scission reactions in the solid state. Macromolecules 1973;6(2):230–5.
[25] Aleksandrov AP, Kitai MS, Varbanskaya RA. Photochemical autocatalytic propagation reaction of polyene sequences in photodegradation of polyvinyl chloride. Polym Sci U.S.S.R 1988;30(8):1687–96.
[26] Boudenne A, Ibos L, Candau Y, Thomas S, editors. Handbook of multiphase polymer systems. West Sussex: John Wiley & Sons; 2011. Chap. 10.
[27] Ohki Y, Hirai N, Fuse N, Tanaka T, Kohtoh M, Okabe S. Search for adequate biodegradable polymer as an eco-friendly electrical insulating material. Proceedings International Symposium on EcoTopia Science 2007; 488–93.
[28] Bityurin N, Luk'yanchuk BS, Hong MH, Chong TC. Models for laser ablation of polymers. Chem Rev 2003;103:519–52.
[29] Astrath NGC, Astrath FBG, Shen J, Zhou J, Michaelian KH, Fairbridge C, et al. Arrhenius behavior of hydrocarbon fuel photochemical reaction rates by thermal lens spectroscopy. Appl Phys Lett 2009;95:191902.
[30] Currie JA, Bohm GGA, Dole M. Calorimetric detection on free radicals in irradiated polyethylene. Polym Lett 1969;7:535–9.
[31] Schindler A, Harper D. Polylactide. II. Viscosity-molecular weight relationships and unperturbed chain dimensions. J Polym Sci: Polym Chem Ed 1979;17: 2593–9.
[32] Hsu ST, Yao YL. Effect of film formation method and annealing on crystallinity of poly (L-lactic acid) films. Proceedings International Manufacturing Science and Engineering Conference 2011; MSEC2011-50205.
[33] Srinivasan R. Pulsed ultraviolet laser interactions with organic polymers dependence of mechanism upon laser power. Polym Degrad Stab 1993;43: 101–7.
[34] Alexander LE. X-ray diffraction methods in polymer science. New York: John Wiley & Sons; 1969.
[35] Wachsen O, Platkowski K, Reichert KH. Thermal degradation of poly-L-lactide—studies on kinetics, modelling and melt stabilisation. Polym Degrad Stab 1997;57:87–94.
[36] Beamson G, Briggs D. High resolution XPS of organic polymers. Chichester: John Wiley & Sons; 1992.
[37] Butiagin PJ. The decay of free radicals in polymer media. Proceedings International Conference on Chemical Transformations of Polymers 1972; 57–76.